

# A Model for Short- and Long-range Interactions of Migrating Tumour Cell

M. Aubert · M. Badoual · B. Grammaticos

Received: 6 February 2008 / Accepted: 22 September 2008 / Published online: 9 October 2008  
© Springer Science+Business Media B.V. 2008

**Abstract** We examine the consequences of long-range effects on tumour cell migration. Our starting point are previous results of ours where we have shown that the migration patterns of glioma cells are best interpreted if one assumes attractive interactions between cells. Here we complement the cellular automaton model previously introduced by the assumption of the existence of a chemorepellent produced by the main bulk of large spheroids (in the hypoxic/necrotic areas). Visible effects due to the presence of such a substance can be found in the density profiles of cells migrating out of a single spheroid as well as in the angular distribution of cells coming from two close-lying spheroids. These effects depend crucially on the diffusion speed of the chemorepellent. A comparison of the simulation results to experimental data of Werbowetski et al. allows to draw (tentative) conclusions on the existence of a chemorepellent and its properties.

**Keywords** Glioblastoma · Invasion · Cellular automaton · Interactions · Repulsion · Secreted factor

## 1 Introduction

Cell migration plays a most important role in the normal functioning of the organism during its growing, as well as its mature, phases. However, cell migration is also an important factor in tumour growth and metastasis. Although unrestrained proliferation is the principal characteristic of malignant tumours, the invasion of neighbouring tissues ensures their spread. Various mathematical models have been proposed in order to study the importance of cell proliferation and cell migration during tumour growth. The original works of Murray (2003), Tracqui et al. (1995,

---

M. Aubert (✉) · M. Badoual · B. Grammaticos  
IMNC, Université Paris VII-Paris XI, CNRS, UMR 8165, Bât. 104, 91406 Orsay, France  
e-mail: aubert@imnc.in2p3.fr

1995), Woodward (1996), and Burgess et al. (1997), modelled glioma growth in terms of a simple equation. In their model the growth term was associated to an exponential increase of the tumour size while the migration was modelled through a diffusion term. This model (despite its simplicity) and its subsequent refinements, in particular that of Swanson et al. (2000, 2002, 2003, 2004), have shown the fundamental role that cell migration plays in glioblastomas, the most aggressive brain tumour. It has also explained in very simple terms why surgical removal of the tumour often fails: this is due to the growth of invading cells, remaining after the operation. The highly invasive character of gliomas has been largely corroborated by numerous clinical and experimental observations (Giese et al. 2003; Palfi et al. 2004).

The invasiveness of glioma cells is a complex process (for reviews see Demuth and Berens 2004; Nakada et al. 2007), which not only involves the high motility of these cells, resulting from the loss or cessation of normally inhibitory controls, but also the upregulation of genes related to migration. Invasion is dependent on the ability of tumour cells to stimulate an extracellular matrix remodelling, via complex matrix-cell interactions (glioma cells secrete proteolytic enzymes which degrade the extracellular matrix in order to create space to move into) (Mueller et al. 2003). Invasion depends also on short-range and long-range cell interactions. Short-range interactions between glioma cells can be either neighbour-to-neighbour interactions via chemical factors or contact interactions. Neighbour-to-neighbour interactions are mediated by growth factors or cytokines that have a direct effect on glioma invasion by stimulating glioma cell migration in an autocrine and paracrine manner (Demuth and Berens 2004; Feldkamp et al. 1997; Mueller et al. 2003; Tysnes and Mahesparan 2001). Still, the action of these factors is essentially described as local, since cells are sensitive to the substances secreted by themselves or by their neighbours. Adhesion proteins or molecules such as cadherins, connexins (transmembrane proteins that form gap junctions between cells) or contactins account for contact interactions. These interactions are described in the literature as either attractive or repulsive, depending on the studied entity. For example, contactin, which is overexpressed in glioma cells, seems to mediate repulsive effects (Eckerich et al. 2006), whereas for connexins recent experiments have brought into light their adhesion properties, which favour cell attraction (Lin et al. 2002). We recently proposed a mathematical model for the migration of glioma cells *in vitro* where we have shown, by observing migration patterns, that communication by gap junctions is equivalent, in our model, to a high attraction between cells (Aubert et al. 2006, 2008).

Finally, it appears that migration of glioma cells can also be directed by long-range secreted factors, emitted by the glioma cells in the tumour bulk. It has been shown that toxic factors are produced during the process of necrosis and regulate the growth of spheroids (Freyer 1988). Recently, Del Duca et al. (2004), Del Maestro and collaborators (2001), Mueller et al. (2003), Tamaki et al. (1997), and Werbowetski et al. (2004) formulated the hypothesis of the existence of a repellent factor produced by cells submitted to stressful conditions such as competition for oxygen and nutrients. This substance would promote migration through a repellent effect on the cells: this could explain why glioma cells detach and migrate away

from the main tumour bulk following a decreasing concentration of this repellent. The authors of Del Duca et al. (2004), Del Maestro et al. (2001), Tamaki et al. (1997) have developed a three-dimensional model of C6 astrocytoma spheroids placed into a collagen type I gel. They observed that tumour cell invasion increases with the size of the spheroid: invasion is significantly greater for larger spheroids (diameter  $> 700 \mu\text{m}$ ) compared to that for smaller spheroids (diameter  $< 500 \mu\text{m}$ ). The repellent factor would be produced by necrotic/hypoxic (or at least stressful) microregions of the spheroids. As larger spheroids have more extended stressful regions they may secrete a larger quantity of chemorepellent, and this could explain their more invasive behaviour. Moreover, Werbowetski et al. (2004) analysed quantitatively the interaction of two spheroids co-cultures, which allowed them to conclude to the existence of a repellent cue, secreted by the centre of the spheroids. They did not identify the chemorepulsive factor: they analyzed several growth promoting factors and guidance cues, but none showed the expected chemorepulsion effects (Brockmann et al. 2003; Mueller et al. 2003). However, as the interest for the repulsion hypothesis is growing, new investigations are launched and recent studies suggest possible candidates (for instance the Slit/Robo ligand-receptor system (Mertsch et al. 2007), or semaphorin (Rieger et al. 2003)).

In the present work we describe a model for the migration of glioma cells from spheroids, based on a cellular automaton, where short-range interactions as well as long-range effects are taken into account. We complement our previous model (which takes into account only short-range interactions between cells) (Aubert et al. 2006, 2008) with long-range interactions, representing a chemorepellent produced by the centre of the spheroid and which diffuses away from it. Our aim is to study the influence of this repellent on the migration pattern. In particular, we show through “virtual experiments” that it may be possible to draw conclusions on the existence of this repellent and to estimate its diffusion coefficient. We also compare our results to some experimental ones.

## 2 Presentation of the Cellular Automaton Model

In previous publications of ours (Aubert et al. 2006, 2008) we have introduced a two-dimensional cellular automaton model in order to describe the migration of tumour cells subject only to cell–cell interactions. The first ingredient of such a model is its geometry. In the studies just mentioned we have chosen a tessellation of hexagonal cells. The advantage of that choice is that it is as isotropic as one can make a tessellation using regular polygons and moreover its algorithmic definition is particularly simple. However, the symmetry imposed by the hexagons is not always a desirable feature. We were thus, naturally led to a different choice for this study and the obvious one was a Voronoi tessellation. Still, despite the underlying Delaunay triangulation, a Voronoi tessellation based on a random collection of points on the plane would have been inadequate, leading to an unacceptable variation of the size of each cell. We should point out here that in our previous models, and in the present one as well, each site can accommodate a single migrating cell: it is thus of utmost importance that the surface of the elementary polygons not vary much. Moreover in the hexagonal tessellation each

cell had precisely six neighbours. The number of neighbours is essential since it conditions the possible movements of a cell. A badly chosen tessellation would lead to too few neighbours and thus artificially slow kinetics. The solution to these problems we adopted, was to start from the triangulation corresponding to the hexagonal tessellation and perturb the position of each site by a random factor. The resulting Voronoi tessellation has polygons of comparable surface and the distribution of the number of neighbours of each site is a gaussian with a mean equal to six and a variance equal to 1.3.

The centre of the spheroid is represented by a region of the lattice which is fully occupied and which ejects an arbitrarily high number of cells. Once a position in the polygons surrounding the spheroid becomes free, it is immediately occupied by a new cell “ejected from the spheroid”.

## 2.1 The Evolution in the Absence of Chemorepellent

As explained above, a polygon can be occupied by a single cell at each time step. Thus, a cell may move only to a free polygon. At each update of the automaton we define a random order of all ejected cells and then evolve them one after the other. When the position of a cell is to be updated a new position is chosen among its neighbours. If this position is occupied, the cell does not move.

In order to account for cell interactions we introduce rules which condition the motion of a cell with respect to its neighbours. The full details of these rules can be found in (Aubert et al. 2006). We showed that in order to reproduce experimental density profiles, the interaction between cells must be maximal attraction. The origin of this attraction may be attributed to the presence of contact interactions (due to gap junctions) or to a short-range chemical attraction between cells. In the following we assume that local interactions are always present and thus the rules that cells must follow is that they will always move staying in contact with some neighbour.

## 2.2 Introduction of the Chemorepellent

In order to model the presence of a chemorepellent we are going to make a few simplifying assumptions. Since we will be talking about some chemical substance it is mandatory to use a grain much finer than the one used for the description of the cells and it is thus quite reasonable to assume that the diffusion of the chemorepellent is governed by a continuous diffusion equation. Moreover, based on the remark of Werbowetski et al. (2004) that the chemical cue is produced in the anaerobic, possibly necrotic, centre of the spheroid, we simplify the situation by assuming a central point source, obtaining an explicit form for the chemorepellent concentration  $C$ :

$$C = Ae^{-\frac{r^2}{4Dt}}, \quad (1)$$

where  $D$  is the diffusion coefficient of the chemorepellent and  $A$  the overall normalisation that does not play any role. In fact, we assume that the migration of the cells is sensitive to the gradient of the chemorepellent concentration (and not to the absolute value of the concentration). First, the advantage of this assumption is

that the expression of the concentration contains just one adjustable parameter,  $D$ . Secondly, this is the case biologically with a chemoattractant, (for instance growth factors (Brockmann et al. 2003)): in experiments in Boyden chambers, cells migrate in the direction of increasing gradient of the chemoattractant. With a chemorepellent, cells migrate in the direction of decreasing gradient. This is also the hypothesis of Werbowetski et al. (2004) even if they suspect a dependence on the absolute concentration when the latter is high. We assume that the repellent concentrations present in our case are not in this range of values and we thus do not take into account this dependence.

We now explain how the response of the cells to the gradient of the concentration is implemented in our model. In order to determine the motion of a cell we compute the difference in chemorepellent concentration between the cell ( $C_0$ ) and its neighbouring sites ( $C_i$ ) (we evaluate the values of  $C_0$  and  $C_i$  at the exact point of the Delaunay triangulation):  $\Delta_i = C_i - C_0$ . Next we add to  $\Delta_i$  some cutoff value  $B$  and retain only those  $\delta_i = \Delta_i + B$  which are positive. The rationale of this is that a cell can move downhill (chemically speaking) and even somewhat uphill, provided the negative slope is not very steep. We have adjusted the value of  $B$  once and for all by requesting that, after a 24 h evolution, 25% of the possible movements be prohibited by too negative a gradient. Next we define a probability of motion by normalising the  $\delta_i$  by their sum. We obtain thus numbers  $q_i$  between 0 and 1. We assume that a cell will choose a site to move to with probability proportional to  $q_i$  (which in turn is proportional to the value of the gradient corrected by  $B$ ). To sum it up, the gradient of the chemorepellent secreted by the centre of the spheroid represents the macroscopic driving force which directs the migration of cells: cells try to avoid high concentrations of chemorepellent by following the direction of decreasing gradient concentration and thus move preferentially radially away from the centre.

The way to combine the two effects, cell interaction and chemorepellent action, is to start by applying the rules related to the maximum attraction between cells. We choose randomly one site among the sites neighbouring the one of the cell which must move. According to the attraction effect the cell may move only if it stays in contact with one neighbour. If this is not possible the cell does not move. Once the attraction rule is satisfied we verify if the constraint related to the presence of the chemorepellent is also satisfied. Only if this second condition is fulfilled does the cell move to the chosen site. Finally, we introduce a prescription in order to cover the case of cells which happen isolated, i.e. at a site with no neighbour whatsoever. In this case the attraction rule is not operative and the motion takes place according to the rules related to the chemorepellent.

In the following, “with long-range interactions” refers to the situation where both short-range and long-range interactions are present, whereas “without long-range interactions” means that only short-range interactions are present. For the sake of simplicity, we abbreviate “long-range interactions” to “LRI”.

### 2.3 Time Calibration

Time calibration of the cellular automaton is a delicate issue. Our previous studies (Aubert et al. 2006, 2008) have shown that the physical time is linearly related to

both the number of ejected cells and the number of iterations of the automaton. Thus simulation time can be counted in number of iterations as well as in number of ejected cells. We choose to present our results with time expressed as the number of ejected cells, as it is a parameter easily accessible in experiments. As a consequence, diffusion coefficients will be expressed in  $\mu\text{m}^2/\text{ejected cell}$ . In order to compare our results with experiments, it is necessary to relate physical time to the number of ejected cells recorded in the experiments in question (cf. Sect. 4.1).

## 2.4 Parameters

The mean lattice size  $a$  is set to  $30\ \mu\text{m}$  (a biologically realistic glioma cell length) and the centre (i.e. the initial spheroid) is composed of the nodes of the Delaunay triangulation that are situated at a smaller distance from the origin of the lattice than  $17a$ .

The question is now how to choose  $D$ . Even if the migration of cells interacting with each other is not a pure diffusion process, we can obtain an effective diffusion coefficient  $D_0$  for migrating cells from our previous model (Aubert et al. 2006, 2008) adapting our analysis to the case of large spheroids just as the ones considered by Werbowetski et al. (2004). From the mean of the square of cell positions as a function of time, we estimate  $D_0 = 0.19 \pm 0.01\ \mu\text{m}^2/\text{s}$ . Despite very different environments, this value is within the range of in vivo value considered by Burgess et al. (1997) ( $10^{-4} - 10^{-3}\ \text{cm}^2/\text{day} \approx 0.1 - 1\ \mu\text{m}^2/\text{s}$ ). With time expressed in number of ejected cells,  $D_0 = 31 \pm 2\ \mu\text{m}^2/\text{ejected cell}$ .

The case of a diffusion coefficient of the repellent  $D$  smaller than  $D_0$  is not physically acceptable since we expect the molecules of the chemorepellent to diffuse faster than the cells. On the other hand, if the diffusion coefficient of the repellent is too large, the concentration profile becomes flat very fast and the repellent does not have any marked influence on the migration of the cells. It turns out that a reasonable value for  $D$  is between  $D_0$  and  $10D_0$  (see Sect. 3.1). In the following, we set  $D = 235\ \mu\text{m}^2/\text{ejected cell} \approx 7D_0$ .

## 3 Results

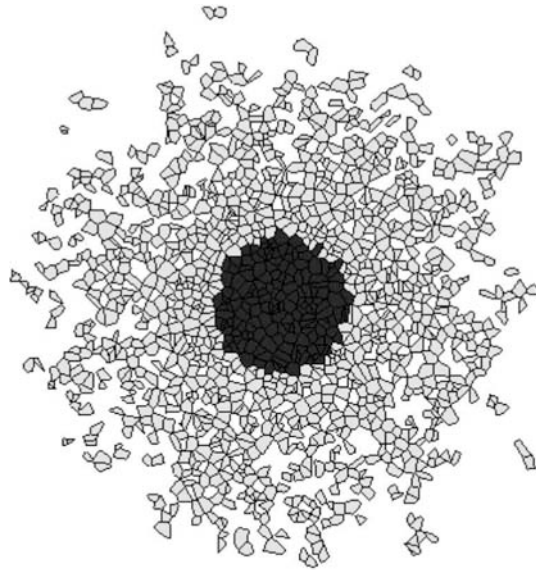
We were inspired by the work of Werbowetski et al. (2004) in order to propose two types of “virtual experiments”. The first consists in studying the growth of one spheroid and we show that precise measurements of cell densities may be sufficient to conclude on the existence of a chemorepellent and even, to evaluate the diffusion coefficient of the repellent. The second type of “virtual experiments” involves two spheroids interacting with each other.

### 3.1 One Spheroid

A typical pattern of migration is presented in Fig. 1.

In order to extract the density profiles of the cell distribution we superimpose on the pattern of the migration, at various numbers of ejected cells, a system of

**Fig. 1** Typical pattern of cell migration ( $t = 1,000$  ejected cells,  $D = 235 \mu\text{m}^2/\text{ejected cell}$ ): cells belonging to the centre are represented in black and grey polygons denote the presence of migrating cells ejected from the spheroid



concentric circles, closely spaced. Calculating densities in this way presents the advantage that the same protocol can be used to calculate experimental densities, from photographs. We then count the number of cells in each circular ring and calculate the density as a function of the distance from the centre of the spheroid. We compare the density profiles with and without long-range interaction, cf. Fig. 2, at the same time (same number of ejected cells).

The density profiles without long-range interactions are roughly linear through the whole range of distances. In the presence of the repellent, the density curves exhibit a more complex, roughly piecewise linear profile with a visible change in slope around  $330 \mu\text{m}$  at 200 ejected cells,  $490 \mu\text{m}$  at 600 ejected cells and  $690 \mu\text{m}$  at 1,000 ejected cells. The comparison with the real position of the maximum of the gradient gives a mean error of  $\pm 15 \mu\text{m}$  (Fig. 3). Before the position of the maximum of the repellent gradient, cell density is higher than in the case without LRI, because cells are repelled from the centre of the spheroid. Beyond the position of the maximum, the cells have not been yet submitted to the highest values of the gradient, and are thus less repelled, which explains the smaller values of cell density in this area. The change in the slope is defined as the intersection point between the two parts of the linear fit, cf. insert in Fig. 2. The existence of a change in the slope of the density curve is an evidence for the existence of a chemorepellent and this property could be used in the analysis of experimental data to support (if observed) the presence of a chemorepellent acting through its gradient.

It is possible to go further in the analysis of the density curve in the presence of a chemorepellent, in order to obtain quantitative results. As explained above, the change in the slope of the density curve is the signature of the presence of a chemorepellent gradient, and the position of this change is close to the position of the maximum of the gradient. As the position of the maximum varies as  $r^2 = 2Dt$ ,

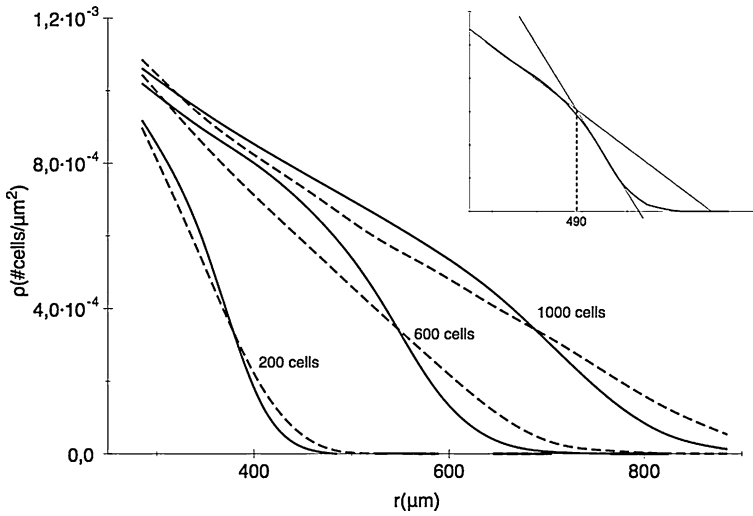


**Fig. 2** Density profiles (200, 600 and 1,000 ejected cells). The dashed lines represent results without long-range interaction and the full lines the density curves with long-range interactions ( $D = 235 \mu\text{m}^2/\text{ejected cell}$ ). For the sake of clarity, the error bars are not represented (the errors amount to a few percent)

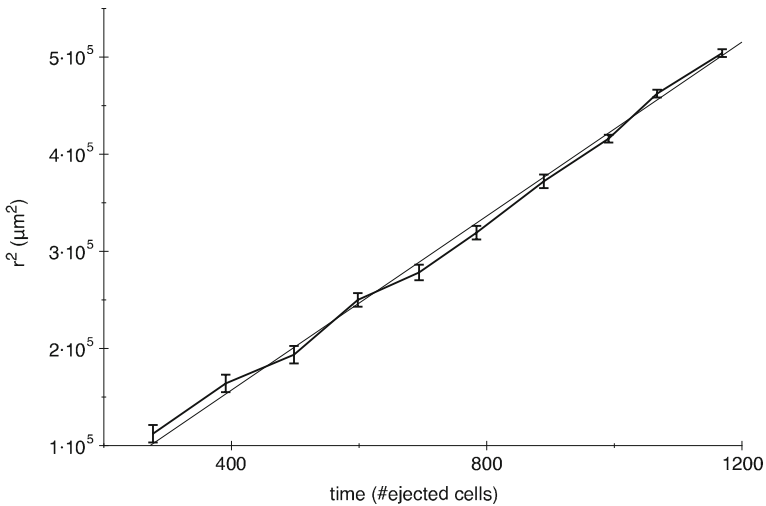


**Fig. 3**  $r^2$  as a function of the number of ejected cells. The error bars come from the error in the location of the change in the slope (determined by the two-part linear fit as explained above). The fit gives  $D = 224 \pm 15 \mu\text{m}^2/\text{ejected cell}$

one can deduce the diffusion coefficient of the chemorepellent from the slope of the linear fit of the curve giving the square of the position against time (Fig. 3).

In Fig. 3 we obtain  $D = 224 \pm 15 \mu\text{m}^2/\text{ejected cell}$ , which is close to the diffusion coefficient parameter chosen in simulations ( $D = 235 \mu\text{m}^2/\text{ejected cell}$ ). For a diffusion coefficient larger than a threshold  $D_{\text{max}}$  the diffusion of the repellent

is too rapid and does not have any marked effect on the migration of the cells. To estimate this value, we assume that the furthest lying cells are located around  $r_0 + 2\sqrt{2D_0t}$  where  $r_0$  is the radius of the spheroid.  $D_{\max}$  satisfies the condition 2:

$$\sqrt{2D_{\max}t} = r_0 + 2\sqrt{2D_0t}. \quad (2)$$

With  $D_0 = 33 \mu\text{m}^2/\text{ejected cell}$ ,  $r_0 = 285 \mu\text{m}$  and  $t = 1,000$  ejected cells, we find  $D_{\max} \approx 320 \mu\text{m}^2/\text{ejected cell}$ , which corresponds to what we observe in simulations. Therefore, for a value of  $D$  larger than  $D_{\max} \approx 10D_0$  the change in the slope is no longer visible.

We can conclude that, if  $D < 10D_0$ , this method provides a reliable estimation of the diffusion coefficient of the chemorepellent secreted by the centre of the spheroid. However, it may be tricky to localize precisely the change in the slope of density profiles. We thus propose another virtual experiment, with two spheroids, where the qualitative signature of a chemorepellent may be more visible in experiments.

### 3.2 Two Spheroids

In this virtual experiment, two spheroids are placed at a given fixed distance ( $d$  is the distance between the two surfaces of the spheroids), eject cells and interact with each other. This type of protocol is also inspired by the work of Werbowetski et al. (2004). In this case, the cell distribution after migration is no longer isotropic. To analyze precisely this anisotropy, we define (on each spheroid) four quadrants A, B, C, and D. The two quadrants that face each other are quadrants A. Opposite to quadrant A in each spheroid is quadrant C. On the sides, quadrants B and D play the same role, due to the axial symmetry of the system. In the following, any reference to the number of cells in quadrant B is a shortcut for the mean of the number of cells in quadrants B and D (cf. Fig. 4a).

In this configuration, the cells of each spheroid not only feel the chemorepellent secreted by their own spheroid, but also by the opposite one. We thus assume that cells are sensitive to the gradient of the total concentration of chemorepellent represented in Fig. 4b (for two different times). Parallely, they can locally interact with cells from their own spheroid as well as with cells coming from the opposite one. Naturally, rules for cell movements with local interactions are the same in both cases, as cells cannot distinguish between cells from their spheroid or from the other one.

If the spheroids are too close (0–200  $\mu\text{m}$  apart), the space between them will be filled quickly in both cases (with and without repellent) and the effect of the chemorepellent will be hardly visible. The larger the distance, the flatter the gradient will be when reaching the other spheroid. Finally, a good compromise is to set the distance between 300 and 600  $\mu\text{m}$ .

The patterns of migration are different with a secreted chemorepellent present or not. The two spheroids after migration ( $t = 750$  ejected cells) are represented in Fig. 5a, b, together with the corresponding density profiles (Fig. 5c, d). In the case of only short-range interactions, cells from the two spheroids coexist not only in the whole area between the two spheroids, which corresponds to quadrant A, but also in

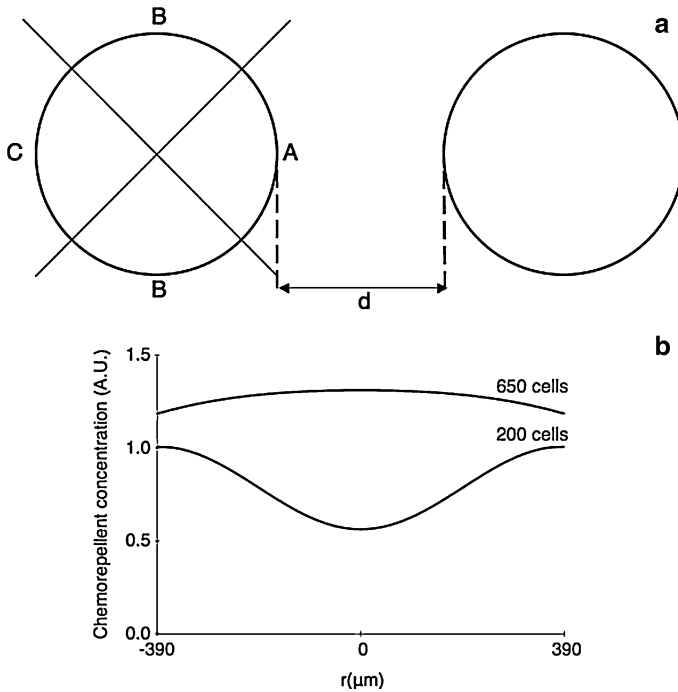


**Fig. 4** **a** Schematic representation of the different quadrants (A, B and C) of the spheroid close to another one (at a distance  $d$  apart) and **b** concentration of the simulated chemorepellent ( $D = 235 \mu\text{m}^2/\text{ejected cell}$ ) felt by the cells in the quadrants A between the two spheroids at time  $t = 200$  and 650 ejected cells ( $d = 300 \mu\text{m}$ ) (“A.U.” = Arbitrary Unit)

quadrant B (cf. Fig. 5b, d). On the contrary, when the centres of the spheroids secrete some chemorepellent ( $D = 235 \mu\text{m}^2/\text{ejected cell}$ ), the cells from the two spheroids barely interpenetrate and the common zone is reduced to a width of 2–3 cells (cf. Fig. 5a, c). Cells from one spheroid are repelled by the chemorepellent secreted by the other spheroid (Fig. 4b).

As they face each other, the two quadrants A are the first to see their cell number affected by the presence of a second spheroid, whereas cell numbers in quadrant C stay relatively unaffected and play a role of reference. We thus analyse the evolution of the difference in the cell number between quadrant C and A ( $C-A$ ) as a function of time (Fig. 6a). At large times ( $>800$  ejected cells) ( $C-A$ ) is clearly larger with LRI than without. With LRI, the chemorepellent diffuses faster than the cells and reaches the cells of the other spheroid earlier. The chemorepellent secreted by the first spheroid slows down the cells of the second one (principally the ones from quadrant A) and cells are trapped in the gradient-flat zone between the two spheroids (see Fig. 4b). As cells cannot overstep the middle point between the spheroids, the number of cells in quadrant A stagnates (and ( $C-A$ ) increases) before quadrant A becomes completely full.

We define  $T_{C=A}$  as the time interval during which the number of cells in quadrant A is the same as in quadrant C (Fig. 6a). In Fig. 6b, we plot  $T_{C=A}$  as a function of the

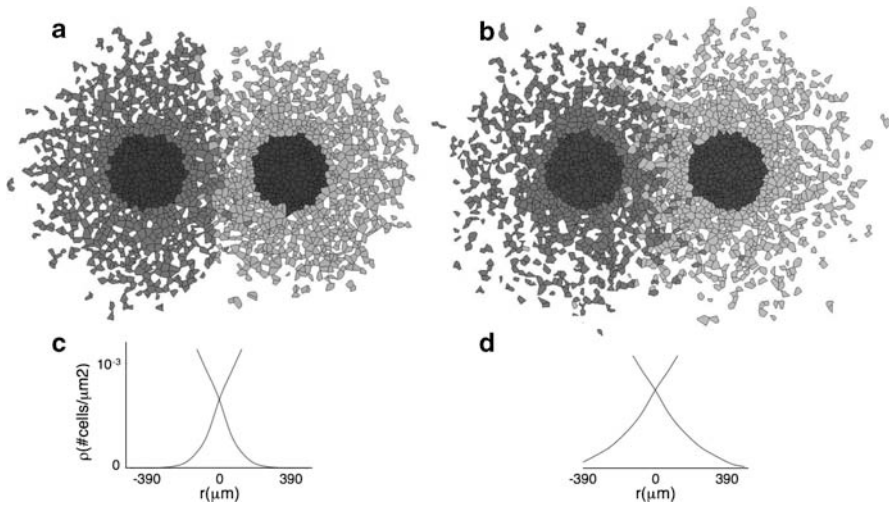


**Fig. 5** Two typical patterns of migration of cells from two adjacent spheroids and the corresponding density profile of cells in quadrant A ( $t = 750$  ejected cells per spheroid) with (a and c) and without chemorepellent (b and d). Distance between the two spheroids:  $300 \mu\text{m}$ . Cells belonging to the centre are represented in black, dark grey polygons denote the presence of migrating cells ejected from the first spheroid (on the left) and light grey polygons denote the presence of migrating cells ejected from the second spheroid (on the right)

distance between the spheroids. We can notice that for small distances, from  $30$  to  $200 \mu\text{m}$ ,  $T_{C=A}$  is comparable with and without LRI: the restricted space between the spheroids is filled before the cells can feel the effects of the chemorepellent. It is thus necessary to place the two spheroids at a distance larger than  $200 \mu\text{m}$  in order to distinguish the cases with and without LRI. For distances larger than  $200 \mu\text{m}$ ,  $T_{C=A}$  is always smaller with LRI than without (Fig. 6b), as seen on Fig. 6a. This qualitatively different behaviour with and without LRI could help distinguish in experiments whether a chemorepellent is secreted or not.

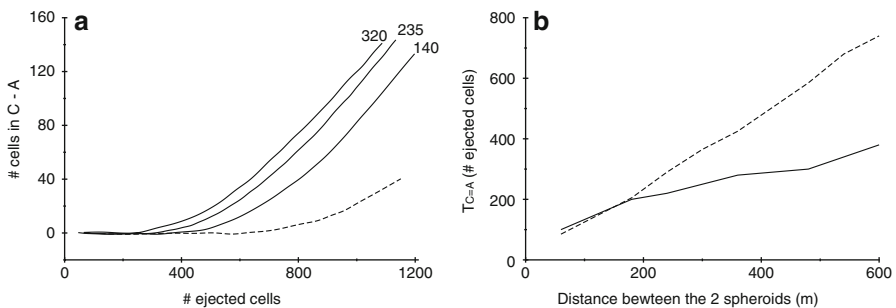


**Fig. 6** a ( $C-A$ ) as a function of number of ejected cells for  $d = 600 \mu\text{m}$  with (full lines,  $D = 140, 235$  and  $320 \mu\text{m}^2/\text{ejected cell}$ ) and without (dashed line) chemorepellent. b  $T_{C=A}$  (time interval during which the number of cells in quadrants A is the same as in quadrant C) as a function of the distance (from  $30$  to  $600 \mu\text{m}$ ) between the two spheroids with (full line,  $D = 235 \mu\text{m}^2/\text{ejected cell}$ ) and without (dashed line) chemorepellent

## 4 Comparison with Experiments

Data in the literature on this subject are scarce. Only the group of Del Maestro has performed experiments to test the hypothesis of a chemorepellent produced by spheroids. Werbowetski et al. (2004) concluded to the existence of a chemorepellent based on their data. Their experiments correspond to the two cases described in the previous section, i.e. the single spheroid and the two spheroid experiments. However, while they acknowledge its existence, they do not give a precise estimate of its diffusion coefficient. Since they report a significant effect between 250 and 600  $\mu\text{m}$  at 48 h, a rough estimate gives  $D$  between 40 and 260  $\mu\text{m}^2/\text{ejected cell}$ .

In this section, after calibrating the model, we compare our results to experimental data in the cases of one and two spheroids. We present the results with and without LRI and we show that it is possible to conclude on the existence of a chemorepellent when the value of the diffusion constant is close to that of the cells. We will see that it is possible to obtain a more precise estimate of the diffusion coefficient of the chemorepellent.

### 4.1 Calibration of the Model

We establish the correspondence between physical time and numbers of ejected cells in experiments with one spheroid and with two spheroids, cf. Table 1. In simulations, the final number of ejected cells coincides with the experimental number of ejected cells. Experimental spheroids have a diameter of 450–600  $\mu\text{m}$ . As the mean lattice size is set to 30  $\mu\text{m}$ , we take a centre of 17–18 cells.

### 4.2 One Spheroid

From the data for Werbowetski et al. (2004) we plot the density of migrating cells as a function of distance for 48 h (1,070 ejected cells, cf. Table 1). In Fig. 7 we compare the experimental density profile with the simulated ones, with and without LRI. The change in slope, which is a signature of the presence of chemorepellent, is clearly visible on the experimental density profile at 48 h, at a distance  $r = 660 \mu\text{m}$ . Moreover, there exists a very good agreement between the experimental density curve at 48 h with the simulated one, when we introduce LRI ( $D = 220 \mu\text{m}^2/\text{ejected}$

**Table 1** Number of ejected cells as a function of time for single spheroid experiments and as a function of time and distance between the two spheroids for two spheroids experiments

A single spheroid		Two spheroids		
Time (hours)	Number of ejected cells	Time (hours)	Distance $d$ between the two spheroids ( $\mu\text{m}$ )	Number of ejected cells
24	270	24	0–100	190
			100–200	295
48	1,070	48	250–400	690
			400–600	770

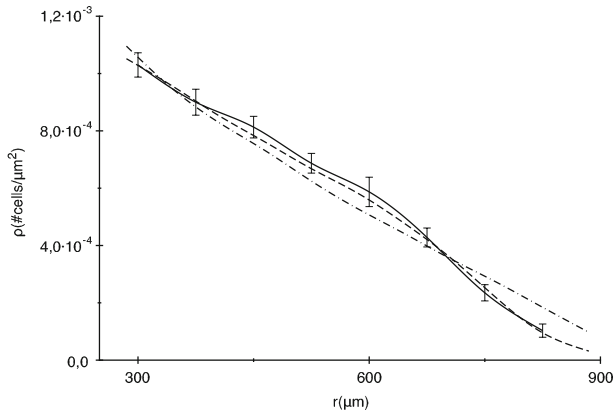


**Fig. 7** Density profiles at 48 h. The full line with error bars is the experimental one. The dashed curve represents simulated density with LRI ( $D = 220 \mu\text{m}^2/\text{ejected cell}$ ) and the dot-dash curve is the simulated density without LRI

cell) in our model (Fig. 7). The agreement is still acceptable for a range of  $\pm 30 \mu\text{m}^2$ /ejected cell around  $D = 220 \mu\text{m}^2/\text{ejected cell}$ . The simulated density curve without LRI (dot-dash line in Fig. 7) has a clearly different shape, more linear, and does not fit the experimental data. More experiments are needed in order to plot  $r^2$  (the squared value of the distance from the origin of the point where the change in slope occurs) versus time and deduce from experiments a more precise value of the diffusion coefficient of the chemorepellent as explained in Sect. 3.1.

### 4.3 Two Spheroids

Next, the authors of (Werbowetski et al. 2004) placed two spheroids close to each other (at distances varying from 0 to  $600 \mu\text{m}$ ) and observed the influence of the presence of a spheroid on the cells coming out from the other. For single spheroids, there was no significant difference between the four quadrants. These results confirm the isotropic cell migration in absence of a second spheroid. However, when the two spheroids are present the migration becomes highly non isotropic, as in the simulations cf. Sect. 3.2. First, the patterns of migration obtained by Werbowetski et al. (2004) correspond to the situation with a chemorepellent, since the authors observed that the two facing spheroids hardly interpenetrate. They picture the situation as that of a wall at the middle between the spheroids, where cells would bump into and never go through. This is close to the pattern of Fig. 6 in simulations with LRI.

For the sake of coherence in simulations, we set  $D$  to the value which corresponds best to the case of a single spheroid, i.e.  $D = 220 \mu\text{m}^2/\text{ejected cell}$ . We compare the experimental and simulated number of cells in the different quadrants as a function of time and distance between the spheroids, cf. Fig. 8. The simulation results with LRI are very close to the experimental ones, cf. Fig. 8, both at 24 h and at 48 h. At 24 h, the steric effect overcomes the influence of the chemorepellent. As observed in simulations (see Sect. 3.2.2), for small distances ( $d < 200 \mu\text{m}$ ) the area

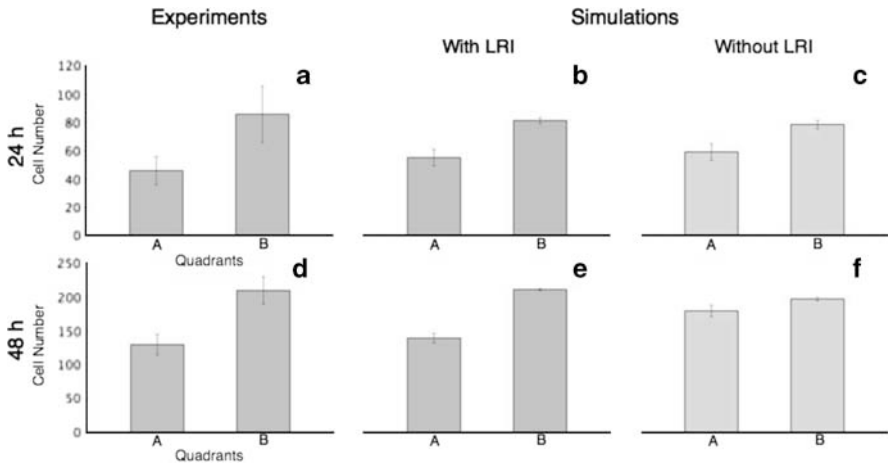


**Fig. 8** Cell numbers in quadrants A and B at 24 h (a–c) ( $100 < d < 200 \mu\text{m}$ ) and 48 h (d–f) ( $450 < d < 600 \mu\text{m}$ ). (a, d) Experimental results taken from Werbowetski et al. (2004). (b, e) Simulations with LRI,  $D = 220 \mu\text{m}^2/\text{ejected cell}$ . (c, f) Simulations without LRI

between the two spheroids is rapidly saturated, and there is no room for new cells. As a consequence, cells cannot detach themselves from the spheroids. The effect is the same with and without chemorepellent. At 48 h, the difference between the two cases of simulations is better visible: the cell number in quadrant A is smaller with LRI. The physical effect related to the number of free sites is not sufficient here in order to reproduce experimental data (Fig. 8d, f). Long-range interactions (with  $D = 220 \mu\text{m}^2/\text{ejected cell}$ ) must be introduced for a better fit of experimental data (Fig. 8d, e). This second set of experiments tends to confirm the existence of a secreted chemorepellent.

## 5 Discussion

The migration of glioma cells is largely influenced by interactions between cells and with the extracellular matrix (or with the substrate for in vitro experiments). In addition, migration can also be directed by diffusive substances emitted by the tumour bulk (or by the centre of the spheroid if in vitro). For example, toxins secreted by hypoxic or necrotic parts of the centre of the tumour may act as chemorepellent. In this case, the migration of cells is likely to favour directions of decreasing concentrations of repellent. As chemotaxis refers to an attractive gradient, one may talk about negative chemotaxis in the case of a repellent. During the last few years, the focus has been on attractive factors that mediate chemotactic and haptotactic migration. Recently, however, the hypothesis of long-range repulsion stimulated a growing interest (Mertsch et al. 2007; Rieger et al. 2003; Werbowetski et al. 2004). In this article, we presented a model of migration of glioma cells submitted to short- and long-range interactions. Our previous model was based on a cellular automaton and described short-range interactions between cells (Aubert

et al. 2006, 2008). We extended it to include the effect of a repellent, the evolution of which is described by a macroscopic diffusion equation. We developed different “virtual experiments” with one or two spheroids, inspired by the experiments of Werbowetski et al. (2004). We have shown that in both cases, it is in principle possible to conclude on the existence of a chemorepellent and to estimate its diffusion coefficient. Moreover, our model, up to a correct calibration of time as the number of ejected cells, can be adapted to different experimental setups with initial spheroids of different size, with different cell lines or with different substrates (Aubert et al. 2006, 2008).

In this paper, we presented a detailed comparison of our results to experimental ones, from Werbowetski et al. (2004). We obtained a very good agreement between simulations with LRI and experiments, for a value of the diffusion coefficient used in the model  $D = 220 \pm 30 \mu\text{m}^2/\text{ejected cell}$ : the experimental density profile for one spheroid displays the same change in slope as in the simulations and matches perfectly the simulated one. With two spheroids, the simulated numbers of cells in the different quadrants are close to the experimental ones, for 24 h and 48 h. This agreement tends to confirm the existence of a chemorepellent in the experiments and allows to give an estimate of the diffusion coefficient around  $D = 220 \mu\text{m}^2/\text{ejected cell}$  ( $=1.4 \mu\text{m}^2/\text{s}$ ). We also identified the condition under which it is possible to conclude on the existence of a chemorepellent: for a large  $D/D_0$  the maximum of the gradient of the repellent is rapidly beyond the cells, the diffusion is too fast. Thus it can not influence the migration of cells and the chemorepellent has little effect on the pattern of migration.

Roughly, from the Einstein law, in a medium 100–1,000 times more viscous than water (collagen after gelation (Newman et al. 1997)),  $D = 1 \mu\text{m}^2/\text{s}$  corresponds to a diffusing particle radius between 0.2 and 2 nm, which is quite realistic for a small protein or a large molecule. It may appear surprising to have a ratio of only 10 between the diffusion coefficients of the chemorepellent and that of the cells, whereas the ratio between radii is expected to be larger than  $10^3$ . However, one has to keep in mind that while the chemorepellent diffuses passively through the matrix of collagen, this is not the case for cells. Cells migrate actively, interact with the matrix and the neighbouring cells and follow preferential paths. The diffusion coefficient of cells is thus an effective one that may not follow the Einstein law.

A point we would like to discuss is the hypothesis that only large spheroids exhibit stressful microregions that secrete chemorepellent. This could explain why in our previous works (Aubert et al. 2006, 2008) it was not necessary to introduce the effect of a repellent in order to describe the migration of glioma cells: we used relatively small spheroids (diameter: 100–300  $\mu\text{m}$ ) that did not have any extensive hypoxic microregions. Therefore, no repellent factor is secreted, or, at least, not produced in a sufficient quantity to have an effect on the migration of glioma cells. It would be interesting to vary (experimentally) the size of the initial spheroids and test whether there is a limit size under which the chemorepellent has no effect. In the latter case, the shape of the density profile should become roughly linear, just as in the case of simulations of small spheroids with short-range interactions only. We also expect a “linear” profile in the case of a large spheroid, if the repellent is inhibited.

The next point is related to the hypothesis that cells are sensitive to the gradient of the concentration of the repellent and not to its absolute concentration. This is the case for positive chemotropism which is a very common phenomenon influencing cell migration during development, wound healing as well as tumour invasion, metastasis and angiogenesis. The idea here was thus to postulate a negative chemotaxis. This hypothesis looks realistic, at least for the concentrations present in the experiments, as it is validated a posteriori by the good agreement between experimental and simulation results. Werbowetski et al. (2004) report that a uniform concentration from conditioned medium can also inhibit the migration of cells (Werbowetski et al. 2004), but this may be due to a very high level of absolute concentration. Indeed, it would be straightforward in the model to define a probability of motion of cells depending on the product of the concentration gradient with a second term prohibiting motion over a threshold of absolute concentration. This would not modify any of our conclusions, as we assumed that for the experiments compared to our model the chemorepellent concentration was below this threshold.

Up to now we focused on modelling migration alone, comparing our results to in vitro experiments with a negligible net proliferation (Aubert et al. 2006, 2008;Oliveira et al. 2005). Moreover the team of Del Maestro in (1997) state explicitly that the majority of invading cells are not proliferating (in agreement with the results of (Bernstein et al. 1991; Chicoine and Silbergeld 1995)) and only a minority of them stop invading and form clusters. Still, in order to investigate a possible influence of proliferation we decided to extend our model so as to include this effect. Thus we repeated our simulations with a proliferation rate of the order of 10% per day. We found that the best agreement between simulations with LRI including proliferation and experiments was obtained for a value of the diffusion coefficient close to  $D = 250 \mu\text{m}^2/\text{ejected cell}$ . This last value is to be compared to the one obtained when no proliferation was considered,  $D = 220 \mu\text{m}^2/\text{ejected cell}$ . We remark that the two values are very close. Moreover the density profiles obtained with  $D = 220 \mu\text{m}^2/\text{ejected cell}$  with and without proliferation differ very little. Thus the effect of proliferation (at least for rates of the order of 10%) does not alter our conclusions.

## 6 Outlook

In order to pinpoint the value of the diffusion coefficient of the repellent, we suggest some new experiments consisting in analyzing the density profiles of one spheroid the diffusion coefficient will be deduced from the position of the change in slope, as explained in Sect. 3.1. in particular, density profiles at different times will be necessary to refine the value of  $D$ .

A more important point concerns the modelling of a 3-D experiment by a 2-D automaton. This is justified by the fact that in experiments, once cells are separated from the spheroid edge, they move radially in a horizontal plane rather than vertically through the gel (Del Maestro et al. 2001). The motion of cells is thus well described by a 2-D model. However, a 3-D model of migration will be necessary to

describe the growth of tumours *in vivo*. In that case proliferation is expected to play a major role and thus should be included also.

Looking forward to future work and possible model improvements, it should be noted that here we have incorporated the evolution of the chemorepellent in the simplest way. In spite of a good agreement between experiments and simulations, we do not pretend to describe what really happens biologically. It is possible that a more complex action of the chemorepellent would lead to the same results. We just proposed one possible scenario, but one has to bear in mind the underlying hypothesis and simplifications. What would possibly lead to different results, would be to take a more complex shape of the repellent source inside the centre of the spheroid: in our model, we made the hypothesis that the repellent is secreted by a source point, as we assumed that hypoxic zone is much smaller than the spheroid and situated at its centre. In future work we intend to consider on one hand a large source (Tamaki et al. (1997) observe that the invasion distance and rate of invasion are significantly increased for larger spheroids) and on the other hand, several sources away from the centre, in order to describe a more realistic situation. Real tumours are far less isotropic than spheroids and several hypoxic regions can develop at different times, not necessarily at the centre of the tumour.

**Acknowledgement** The authors are indebted to G. d'Avout for his help at the initial stages of this work.

## References

- Aubert M, Badoual M, Fereol S, Christov C, Grammaticos B (2006) A cellular automaton model for the migration of glioma cells. *Phys Biol* 3:93–100
- Aubert M, Badoual M, Christov C, Grammaticos B (2008) A model for glioma cell migration on collagen and astrocytes. *J R Soc Interface* 5:75–83
- Bernstein JJ, Laws ER Jr, Levine KV, Wood LR, Tadvalkar G, Goldberg WJ (1991) C6 glioma-astrocytoma cell and fetal astrocyte migration into artificial basement membrane: a permissive substrate for neural tumors but not fetal astrocytes. *Neurosurgery* 28:652–658
- Brockmann MA, Ulbricht U, Grüner K, Fillbrandt R, Westphal M, Lamszus K (2003) Glioblastoma and cerebral microvascular endothelial cell migration in response to tumor-associated growth factors. *Neurosurgery* 52:1391–1399
- Burgess PK, Kulesa PM, Murray JD, Alvord EC Jr (1997) The interaction of growth rates and diffusion coefficients in a three-dimensional mathematical model of gliomas. *Neuropathol Exp Neurol* 6:704–713
- Chicoine MR, Silbergeld DL (1995) Assessment of brain tumor cell motility *in vivo* and *in vitro*. *J Neurosurg* 82:615–622
- Del Duca D, Werbowetski T, Del Maestro R (2004) Spheroid preparation from hanging drops: characterization of a model of brain tumour invasion. *J Neurooncol* 67:295–303
- Del Maestro R, Shivers R, McDonald W, Del Maestro A (2001) Dynamics of C6 astrocytoma invasion into three-dimensional collagen gels. *J Neurooncol* 53(2):87–98
- Demuth T, Berens ME (2004) Molecular mechanisms of glioma cell migration and invasion. *J Neurooncol* 70:217–228
- Eckerich C, Zapf S, Ulbricht U, Müller S, Fillbrandt R, Westphal M, Lamszus K (2006) Contactin is expressed in human astrocytic gliomas and mediates repulsive effects. *Glia* 53:1–12
- Feldkamp MM, Lau N, Guha A (1997) Signal transduction pathways and their relevance in human astrocytomas. *J Neurooncol* 35:223–248
- Freyer JP (1988) Role of necrosis in regulating the growth saturation of multicellular spheroids. *Cancer Res* 48:2432–2439

- Giese A, Bjerkvig R, Berens ME, Westphal M (2003) Cost of migration: invasion of malignant gliomas and implications for treatment. *J Clin Oncol* 21(8):1624–1636
- Lin JH, Takano T, Cotrina ML, Arcuino G, Kang J, Liu S, Gao Q, Jiang L, Li F, Lichtenberg-Frate H, Haubrich S, Willecke K, Goldman SA, Nedergaard M (2002) Connexin 43 enhances the adhesivity and mediates the invasion of malignant glioma cells. *J Neurosci* 23:4302–4311
- Mertsch S, Schmitz N, Jeibmann A, Geng JG, Paulus W, Senner V (2007) Slit2 involvement in glioma cell migration is mediated by Robo1 receptor. *J Neurooncol* (on line at <http://www.springerlink.com/content/krm4211443579053/>)
- Mueller MM, Werbowetski T, Del Maestro RF (2003) Soluble factors involved in glioma invasion. *Acta Neurochir (Wien)* 145:999–1008
- Murray JD (2003) *Mathematical biology II: spatial models and biomedical applications*, 3rd edn. Springer-Verlag, Berlin-Heidelberg-New York, pp 536–613
- Nakada M, Nakada S, Demuth T, Tran NL, Hoelzinger DB, Berens ME (2007) Molecular targets of glioma invasion. *Cell Mol Life Sci* 64:458–478
- Newman S, Clotre M, Allain C, Forgacs G, Beysens D (1997) Viscosity and elasticity during collagen assembly in vitro: relevance to matrix-driven translocation. *Biopolymers* 3:337–347
- Oliveira R, Christov C, Guillamo J S, de Bouard S, Palfi S, Venance L, Tardy M, Peschanski M (2005) Contribution of gap junctional communication between tumor cells and astroglia to the invasion of the brain parenchyma by human glioblastomas. *BMC Cell Biol* 6:7–24
- Palfi S, Swanson KR, De Bouard S, Chretien F, Oliveira R, Gherardi RK, Kros JM, Peschanski M, Christov C (2004) Correlation of in vitro infiltration with glioma histological type in organotypic brain slices. *Br J Cancer* 91(4):745–752
- Rieger J, Wick W, Weller M (2003) Human malignant glioma cells express semaphorins and their receptors, neuropilins and plexins. *Glia* 42(4):379–389
- Swanson KR, Alvord EC Jr, Murray JD (2000) A quantitative model for differential motility of gliomas in grey and white matter. *Cell Prolif* 33:317–329
- Swanson KR, Alvord EC Jr, Murray JD (2002) Virtual brain tumours (gliomas) enhance the reality of medical imaging and highlight inadequacies of current therapy. *Br J Cancer* 86:14–18
- Swanson KR, Bridge C, Murray JD, Alvord ED Jr (2003) Virtual and Real Brain Tumors: Using Mathematical Modeling to Quantify Glioma Growth and Invasion. *J Neurol Sci* 216:1–10
- Swanson KR, Alvord EC Jr, Murray JD (2004) Dynamics of a model for brain tumors reveals a small window for therapeutic intervention. *Discrete and Continuous Dynamical Systems Series B* 4:289–295
- Tamaki M, McDonald W, Amberger VR, Moore E, Del Maestro RF (1997) Implantation of C6 astrocytoma spheroid into collagen type I gels: invasive, proliferative, and enzymatic characterizations. *J Neurosurg* 87(4):602–609
- Tracqui P (1995) From passive diffusion to active cellular migration in mathematical models of tumour invasion. *Acta Biotheor* 43:443–464
- Tracqui P, Cruywagen GC, Woodward DE, Bartoo GT, Murray JD, Alvord EC Jr (1995) A mathematical model of glioma growth: the effect of chemotherapy on spatio-temporal growth. *Cell Prolif* 28:17–31
- Tysnes BB, Mahesparan R (2001) Biological mechanisms of glioma invasion and potential therapeutic targets. *J Neurooncol* 53:129–147
- Werbowetski T, Bjerkvig R, Del Maestro RF (2004) Evidence for a secreted chemorepellent that directs glioma cell invasion. *J Neurobiol* 60(1):71–88
- Woodward DE, Cook J, Tracqui P, Cruywagen GC, Murray JD, Alvord EC Jr (1996) A mathematical model of glioma growth: the effect of extent of surgical resection. *Cell Prolif* 29:269–288